One-dimensional spin-polarized surface states: A comparison of Bi(112) with other vicinal bismuth surfaces

Anna Cecilie Åsland[1], Johannes Bakkelund[1], Even Thingstad[1,2], Håkon I. Røst[1,3], Simon P. Cooil[4], Jinbang Hu[1], Ivana Vobornik[5], Jun Fujii[5], Asle Sudbø[1], Justin W. Wells[1,4,*] and Federico Mazzola[5]

[1]*Department of Physics, Norwegian University of Science and Technology (NTNU), NO-7491 Trondheim, Norway*
[2]*Department of Physics, University of Basel, Klingelbergstrasse 82, CH-4056 Basel, Switzerland*
[3]*Department of Physics and Technology, University of Bergen, NO-5007 Bergen, Norway*
[4]*Centre for Materials Science and Nanotechnology, University of Oslo, Oslo 0318, Norway*
[5]*Istituto Officina dei Materiali (IOM)-CNR, Area Science Park-Basovizza, S.S. 14 Km 163.5, 34149 Trieste, Italy*

Vicinal surfaces of bismuth are unique test beds for investigating one-dimensional (1D) spin-polarized surface states that may one day be used in spintronic devices. In this paper, such states have been observed for the (112) surface when measured using angle- and spin-resolved photoemission spectroscopy, and also when calculated using a tight-binding model and with density functional theory. The surface states appear as elongated Dirac-cones which are 1D and almost dispersionless in the $\mathbf{k}_y$ direction, but disperse with energy in the orthogonal $\mathbf{k}_x$ direction to form two ×-like features centered at the $\mathbf{k}_y$ line through $\bar{\Gamma}$. Unlike many materials considered for spintronic applications, their 1D nature suggests that conductivity and spin-transport properties are highly dependent on direction. The spin polarization of the surface states is mainly in plane and parallel to the 1D states, but there are signs of a tilted out-of-plane spin-vector component for one of the features. The Bi(112) surface states resemble those found for other vicinal surfaces of bismuth, strongly indicating that their existence and general properties are robust properties of vicinal bismuth surfaces. Furthermore, differences in the details of the states, particularly related to their spin polarization, suggest that the electronic band structure may be engineered simply by precise cutting and polishing of the crystal.

I. INTRODUCTION

Finding materials where spin filtering and spin transport can be realized, either through electrical currents or magnon currents, is of major importance in spintronics [1–6]. Spin states facilitating the flow of spin-polarized electrical currents are typically found in heavy element materials like bismuth because of their strong spin-orbit coupling [7–10].

Two surfaces of bismuth, Bi(441) and Bi(114), have previously been found to support one-dimensional (1D), spin-polarized surface states [11,12]. The one-dimensionality of these states suggests that conductivity and spin transport can vary along different directions on the surface. This distinguishes them from many topological insulators for which conductivity and spin-transport properties tend to be closer to isotropic [13–16]. Furthermore, the spin polarization of the surface states on Bi(441) and Bi(114) makes backscattering of surface state electrons less likely, since this implies a full reversal of their spin vectors [3–5]. Another advantage of pure bismuth is how easy it is to cut, polish, and clean compared to many topological insulators, which tend to be alloys [13–16]. True vicinal surfaces of alloys are challenging to achieve consistently as the surface stoichiometry, and therefore the electronic properties, will easily vary upon repreparation.

One of the reasons for the intense interest in topological insulators is that the topology of the surface states protects electrons in these states from scattering, unless the scattering involves a mechanism that allows an exchange of spin angular momentum [3–5,13–16]. Since topological insulators are ideally insulators in the bulk, electrical transport happens through their surface states. Bismuth is a semimetal, so transport can also happen through its bulk states where electrons are not generally protected from scattering, in addition to surface state conduction [8,17]. However, if gaps could be opened in the energy spectrum of bismuth such that only the surface states reside on the Fermi surface or, alternatively, if vicinal surfaces could be achieved on similar topological insulators like $Bi_{1-x}Sb_x$ [5,18,19], they could be prime candidates for anisotropic electrical spin transport. Vicinal surfaces of bismuth are therefore great test beds to investigate the properties of such surface states and how they can be modified. Understanding the underlying physical mechanisms of the electronic and spin structure in a well-known elemental crystal should thus aid the exploration of similar materials which can possibly be used in spin-based devices in the future.

Herein, we show that another vicinal surface of bismuth, Bi(112), exhibits 1D, spin-polarized surface states resembling those found on Bi(441) and Bi(114) [11,12]. Angle-resolved photoemission spectroscopy (ARPES) measurements reveal two spin-polarized ×-like features in the energy spectrum, centered at $\bar{\Gamma}_1$ in the center of the first Brillouin zone (BZ)

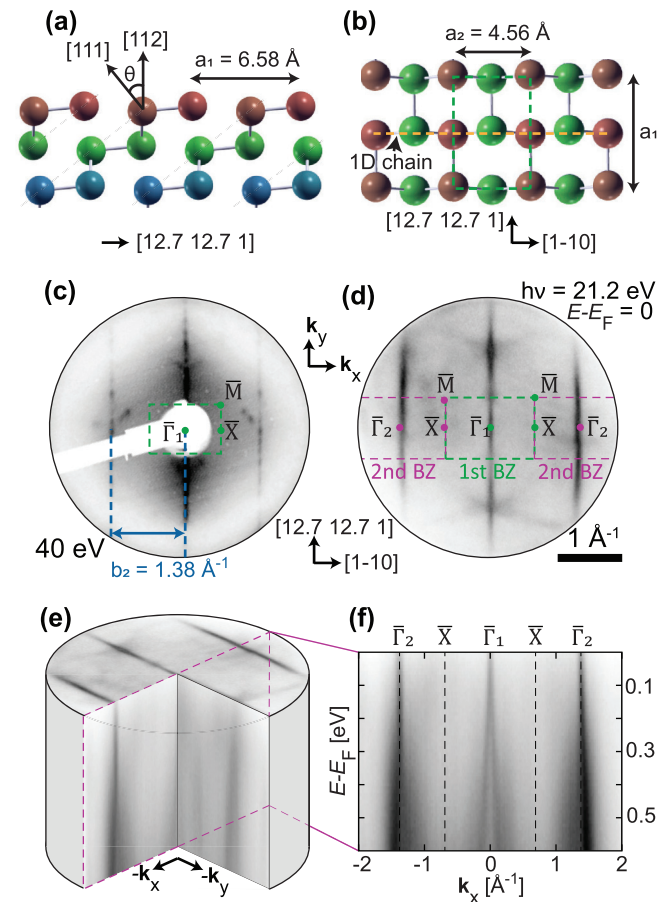*Corresponding author: j.w.wells@fys.uio.no

FIG. 1. The atomic and electronic structure of Bi(112). (a) Sketch showing the atomic structure of the vicinal Bi(112) surface from the side. Red, green, and blue spheres represent the uppermost, second, and third layers of the crystal, respectively. (b) Top view schematic of the Bi(112) surface with the unit cell indicated (green). The $x/\mathbf{k}_x$, $y/\mathbf{k}_y$, and $z/\mathbf{k}_z$ axes correspond to the crystallographic directions [1-10], [12.7 12.7 1], and [112], respectively. (c) Low-energy electron diffraction (LEED) pattern of the Bi(112) surface, measured with an electron energy of 40 eV. The green rectangle shows the first Brillouin zone (BZ). b_2 is the distance between the streaks, and corresponds to the length a_2 of the unit cell along the atomic chains. (d) The two-dimensional Fermi surface of Bi(112). The first and second BZs are indicated by green and purple rectangles, respectively. (e) Volumetric representation of the measured Bi(112) band structure. (f) Measured band structure (E_B vs $\mathbf{k}_x$) at $\mathbf{k}_y = 0$, i.e., orthogonal to the one-dimensional surface states.

[see Fig. 1(d)], with each of their crossing points at approximately the same binding energies (E_B, also known as $E - E_F$) as the surface states of Bi(441) [11]. Similarly, Bi(114) also has a 1D spin-polarized surface state at one of these E_B [12]. Spin-polarized surface states therefore appear to be a robust property of vicinal bismuth surfaces. Interestingly, all three surfaces show subtle differences in the details of their surface states, suggesting that properties like the direction of the spin vector can be tuned simply by cutting the crystal along a given direction. This gives a unique way to explore low-dimensional surfaces and how their electronic properties can be modified.

II. RESULTS AND DISCUSSION

The vicinal surface of Bi(112) can be described by sheets of atoms with edges forming parallel lines on the surface [see Figs. 1(a) and 1(b)]. Due to dimerization, the lines are only weakly coupled. This results in a macroscopic number of parallel quasi-1D systems. The surface structure shown in Figs. 1(a) and 1(b) is confirmed by low-energy electron diffraction (LEED) in Fig. 1(c). The distance between the streaks indicated in Fig. 1(c) matches the periodicity of the truncated bulk crystal in the direction parallel to the 1D atomic chains. This suggests that there is no surface reconstruction along the atomic chain, which is as expected given that charge-density waves are very unlikely when the 1D states are spin polarized [20]. Charge-density waves have been observed as additional 1D streaks in the LEED pattern at low temperature for another vicinal surface of bismuth [21], but no such streaks can be seen for Bi(112). In Fig. 1(c), the streaks appear to consist of several closely spaced spots, seemingly caused by the stacking of the underlying layers [22]. ARPES measurements further confirm the 1D character of the surface-localized electrons. The Fermi surface with 1D states along $\mathbf{k}_y$ is shown in Fig. 1(d). As seen in Figs. 1(e) and 1(f), these lines consist of two bands in each BZ dispersing in energy to form ×-like features, crossing each other at the $\bar{\Gamma}$ points close to the Fermi level. The bands resemble the shape of a Dirac cone, but with the Dirac point elongated to form a "Dirac line" parallel to $\mathbf{k}_y$, and an × in the orthogonal directions along $\pm\mathbf{k}_x$ [22].

To differentiate surface states from bulk states, measurements were performed as a function of photoexcitation energy $h\nu$. Although symmetry breaking in the out-of-plane direction ($\hat{\mathbf{z}}$) caused by the surface means that the out-of-plane momentum ($\propto \mathbf{k}_z$) is not well conserved in the photoemission process, the $\mathbf{k}_z$ dispersion of emitted bulk state electrons can still be probed by varying the excitation energy [23]. On the other hand, surface states are localized on the surface and their energy is therefore independent of $\mathbf{k}_z$ (and $h\nu$) [24].

An overview of the results is given in Fig. 2(a), showing a sketch of the measured surface states (dark blue and light blue), compared to calculated tight-binding (TB) surface (dark pink, light pink and brown) and bulk (green) states. In Figs. 2(b)–2(d) and 2(f)–2(h), the bands at E_B larger than ≈0.3 eV are seen to disperse with photoexcitation energy and are therefore identified as bulk bands. In addition, there are two ×-like features formed by bands crossing each other at $\bar{\Gamma}_1$. One of the ×'s is apparent in Figs. 2(b) and 2(f)–2(h) and is represented by the dark blue bands labeled $\times_{E_F}$ in Fig. 2(a). The other × is visible in Figs. 2(b) and 2(c) and is shown as light blue bands labeled $\times_{0.16\,\mathrm{eV}}$ in Fig. 2(a). These bands do not disperse with photoexcitation energy, hence they are identified as surface states. However, a noticeable variation in intensity is observed, most likely related to photoionisation matrix element effects [23,25]. As indicated by arrows in Fig. 2(a), $\times_{E_F}$ (dark blue) has its crossing point near the Fermi level at $E_B = 0.07 \pm 0.10$ eV. In comparison, $\times_{0.16\,\mathrm{eV}}$ [light blue in Fig. 2(a)] has its crossing point at a larger E_B of $E_B = 0.16 \pm 0.05$ eV, as can be seen from Fig. 2(c) [22].

The electronic structure of Bi(112) was calculated using TB calculations and density functional theory (DFT) [22]. The TB calculations are shown in the left-hand side panel
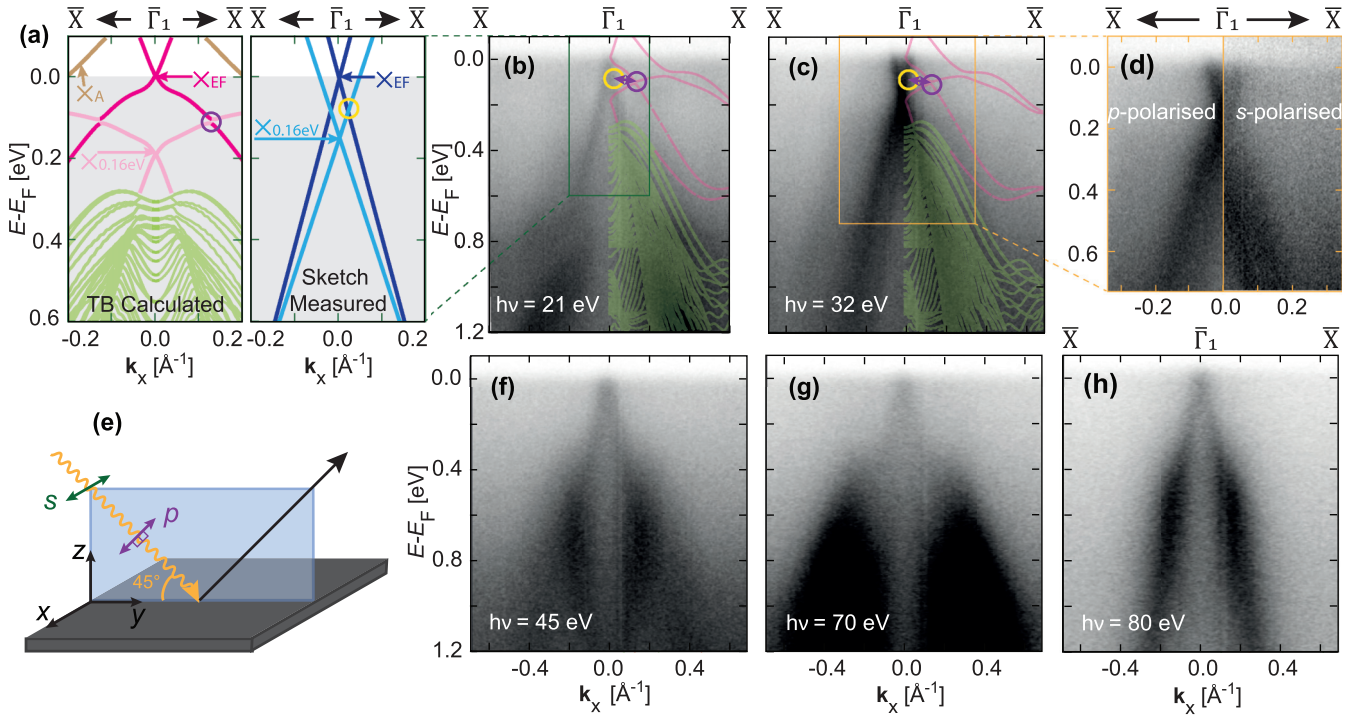
FIG. 2. (a) An overview of the band structure near the $\bar{\Gamma}_1$ point (E_B vs $\mathbf{k}_x$) at $\mathbf{k}_y = 0$. The dark blue and light blue bands represent the two measured ×-like features at $\bar{\Gamma}_1$, where the dark blue bands are clearest in (b) and (f)–(h), and the light blue bands clearest in (c) and (d). The arrows from $\times_{E_F}$ and $\times_{0.16\,eV}$ indicate the crossing points of the ×-like features. The green and pink/brown bands are bulk and surface states, respectively, calculated using a tight-binding (TB) model. The dark pink bands are thought to correspond to $\times_{E_F}$ and the light pink bands to $\times_{0.16\,eV}$ seen in the measurements. The yellow and purple circles show the measured (dark blue cross light blue) and calculated (light pink cross dark pink) crossing of $\times_{E_F}$ and $\times_{0.16\,eV}$, respectively. (b)–(d), (f)–(h) The band structure along $\bar{X} - \bar{\Gamma}_1 - \bar{X}$ measured with photoexcitation energies $h\nu = 21$ eV (b); $h\nu = 32$ eV (c), (d); 45 eV (f); 70 eV (g); and 80 eV (h). In (b)-(c) the TB calculations are overlaid on the measurements. The yellow/purple circles and purple arrow indicate where the ×-like features cross each other in the measurements and calculations. In (d), which is measured inside the orange region in (c), the left-hand side is measured with p-polarized (partly out-of-plane) light, and the right-hand side with s-polarized (in-plane) light. The direction of the light polarization with respect to the sample surface is sketched in (e).

in Fig. 2(a) and overlaid on the measured band structures in Figs. 2(b) and 2(c). The bulk states (green) have been calculated for a range of $\mathbf{k}_z$, hence the measured bulk states are expected to disperse within the area they cover. There is good agreement between the TB calculated (green) and measured bulk states. Similarly, the TB calculated surface states (shades of pink) resemble the two ×-like features in the ARPES measurements, with crossing points at $E_B = -0.032$ eV and $E_B = 0.166$ eV for $\times_{E_F}$ (dark pink) and $\times_{0.16\,eV}$ (light pink), respectively.

Surface-state calculations on complicated surface projections are challenging to perform accurately, and have previously not been possible to perform for vicinal surfaces of bismuth. Although the E_B of the crossing points in the measurements agree within uncertainties with the values expected from calculations, the gradients of the bands differ. Additionally, in the measurements the bands in $\times_{0.16\,eV}$ cross the Fermi level, while in the TB calculations the brown bands labeled $\times_A$ (not seen in the measurements) in Fig. 2(a) cross the Fermi level instead of bands assigned to $\times_{0.16\,eV}$. Below the $\times_{E_F}$ crossing point and above the $\times_{0.16\,eV}$ crossing point, the measured bands are much steeper than the calculated bands. Because of this, the ($\mathbf{k}_x$, E_B) point where the bands extending from $\times_{E_F}$ and $\times_{0.16\,eV}$ are measured to cross

[yellow circle in Figs. 2(a)–2(c)] is at a different value of $\mathbf{k}_x$ and E_B compared to the calculated bands [purple circle in Figs. 2(a)–2(c)]. Although a truncated bulk surface seems to give the best agreement between the measured and calculated band structure, preliminary DFT calculations indicated that surface state gradients and energies are very sensitive to the precise geometry at the surface [26]. Reconstruction of the surface, or missing rows of atoms as observed in Ref. [12], may therefore explain the difference in band gradients, potentially leading to a mechanism to control the surface Fermi velocities. If there is a periodic surface reconstruction, one can expect an altered spin polarization and/or number of Fermi-level crossings, but these details seem to be correctly described by the TB calculations.

A possible missing row reconstruction may also appear to explain the noninteracting nature of the 1D surface states: If the distance between the sheet edges is large, a weak interaction between their constituent electronic states is expected [27]. However, the distance between the sheet edges in Bi(112) (<1 nm) is much smaller than the distances between the 1D gold atomic chains on silicon reported in Ref. [27], for which the interaction between electronic states already appears at distances $\lesssim 2$ nm. Considering the straightness of the 1D lines in the measured band structure of Bi(112), it

TABLE I. A comparison of the binding energies (E_B) of the crossing points and spin vectors of the ×-like features in the measured band structure of three vicinal bismuth surfaces. TB Bi(112) gives the equivalent results from tight-binding calculations. The spin-vector angles are measured relative to the surface plane, thus indicating the magnitude of the out-of-plane spin-vector component.

Surface	E_B Crossing point (eV)		Spin-vector angle (°)	
	$\times_{E_F}$	$\times_{0.16\,\text{eV}}$	$\times_{E_F}$	$\times_{0.16\,\text{eV}}$
Bi(112)	0.07 ± 0.10	0.16 ± 0.05	0	27 ± 7
Bi(441) [11]	≈ 0	$0.15 - 0.20$	0	-45
Bi(114) [12]	$0 - 0.15^{\text{a}}$	Not seen	30	Not seen
TB Bi(112)	-0.032	0.166	≈ 0	≈ 0

^aFor Bi(114), the surface state resembles a single, straight line on top of a Λ-like bulk state. Hence, it is not clear whether the surface state is × like with a crossing point. The maximum E_B in the given range is estimated as the largest E_B of the surface state. See Ref. [12] for further details.

seems likely that this interaction is absent, despite the smaller separation of the edges in real space. One possible explanation is the difference in screening of electrons in the two materials. Bismuth has an electron carrier density on the order of $10^{23}\,\text{cm}^{-3}$, giving a Thomas-Fermi screening length of ≈ 0.05 nm [28,29]. In comparison, the silicon used in Ref. [27] has an electron carrier density on the order of $10^{18}\,\text{cm}^{-3}$, giving a Thomas-Fermi screening length of ≈ 0.3 nm [27,29,30]. Since the screening length in bismuth is small compared to the distance between the 1D chains in Bi(112), the states appear to be noninteracting, even without a surface reconstruction or missing rows on the surface.

Hence, even if surface reconstruction is one possible explanation for the discrepancy between the band gradients, there is no strong evidence for this in the measured ARPES or in the LEED pattern [22]. Overall, even if the shapes of the bands appear somewhat different, the TB calculations predict the two ×-like features with crossing points at E_B in agreement with those observed from the ARPES measurements.

The ×-like features are similar to the surface states observed for other vicinal surfaces of bismuth, as summarized in Table I and in the Supplemental Material [22]. Two ×-like surface-state features with their crossing point near the Fermi level and at $E_B = 0.16 - 0.20$ eV are observed for both the (112) and (441) surface [11]. The measured band structure of Bi(114) has a Λ-shaped bulk feature with its maximum point near $E_B \approx 0.15$ eV, but with an additional 1D surface state at E_B between $0 - 0.15$ eV [12]. For all three surfaces, the one-dimensionality of the surface states is expected to influence the conduction properties. A distinct increase in the conductivity along the atomic rows of the surface when compared to the orthogonal direction is expected, as there are far more states to scatter into along the surface chains [see Fig. 1(b)].

To investigate the orbital origins of the observed states, the polarization of the light was varied between *s* and *p* polarization (in-plane and partly out-of-plane, respectively) as visualized in Fig. 2(e). An example is given in Fig. 2(d), where an additional band can be observed inside the $\times_{0.16\,\text{eV}}$ feature

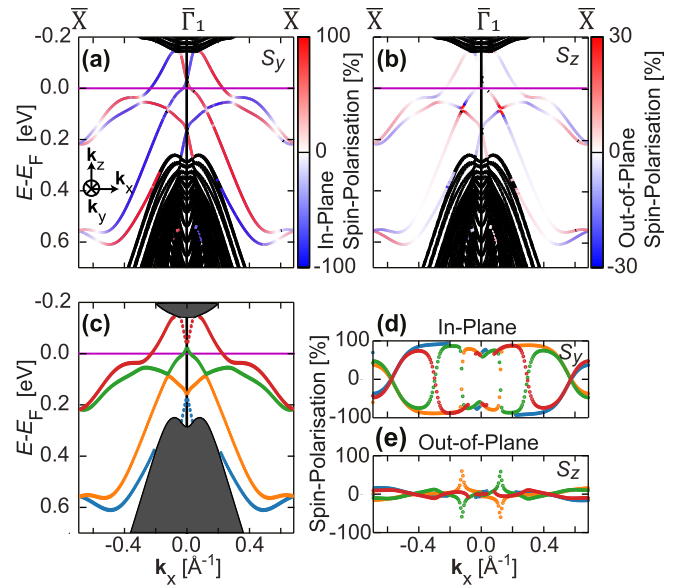

FIG. 3. Spin polarization from tight-binding calculations. (a)–(c) Band structure between $\bar{X} - \bar{\Gamma}_1 - \bar{X}$. In (a) and (b), the color scale shows the spin-polarization $\mathbf{S}_y$, the spin-vector component in plane and along the 1D lines, (a), and $\mathbf{S}_z$, the out-of-plane component of the spin vector, (b). Note that the color scale is different between (a) and (b). In (c), the colors label the surface bands. (d), (e) Spin-polarization of the spin-vector component $\mathbf{S}_y$ (d) and $\mathbf{S}_z$ (e), respectively. The color shows which band in (c) the spin-polarization value belongs to.

when measured with *s*-polarized light (right-hand side panel). Since this is in the region where bulk bands are found from the calculations, it is believed to be a bulk band [22].

Due to the strong spin-orbit coupling in bismuth, the surface states are expected to be spin polarized [7,8]. This is demonstrated in Fig. 3, showing the TB calculated spin-polarization dependence of the surface states. Positive (negative) spin polarization shown in red (blue) gives the magnitude of the spin-vector component in plane and pointing along $+\mathbf{k}_y$ ($-\mathbf{k}_y$), $\mathbf{S}_y$, in Fig. 3(a) and out of plane pointing along $+\mathbf{k}_z$ ($-\mathbf{k}_z$), $\mathbf{S}_z$, in Fig. 3(b). For all the surface bands, $\mathbf{S}_y$ is close to $\pm 100\%$ [Figs. 3(a) and 3(d)]. The exception is the points where the surface states in $\times_{0.16\,\text{eV}}$ intersect those in $\times_{E_F}$ [yellow/purple circles and purple arrow in Figs. 2(a)–2(c)]. There, the said states also attain a significant out-of-plane spin-vector component $\mathbf{S}_z$ [Figs. 3(b) and 3(e)].

The measured in-plane spin-polarization shown in Fig. 4 is consistent with the calculations in Fig. 3. The spin-ARPES measurements were performed using a range of photoexcitation energies, with *s*, *p*, and unpolarized light, and at different polar (θ) and azimuthal (φ) angles [22]. Because of the consistent spin polarization in these different measurements and the consistency with the calculated spin polarization, the measured spin is considered to represent the spin polarization of the initial state (see further details in the Supplemental Material). In Figs. 4(a) and 4(b), constant energy surfaces are shown at $E_B = 0.12$ eV and $E_B = 0.72$ eV. At both energies, the region spanned by the entire first BZ (green, dashed rectangle) has been filled with the measured projection of the spin vector in-plane and along $\pm\mathbf{k}_y$ (i.e., $\mathbf{S}_y$). At $E_B = 0.12$ eV, the
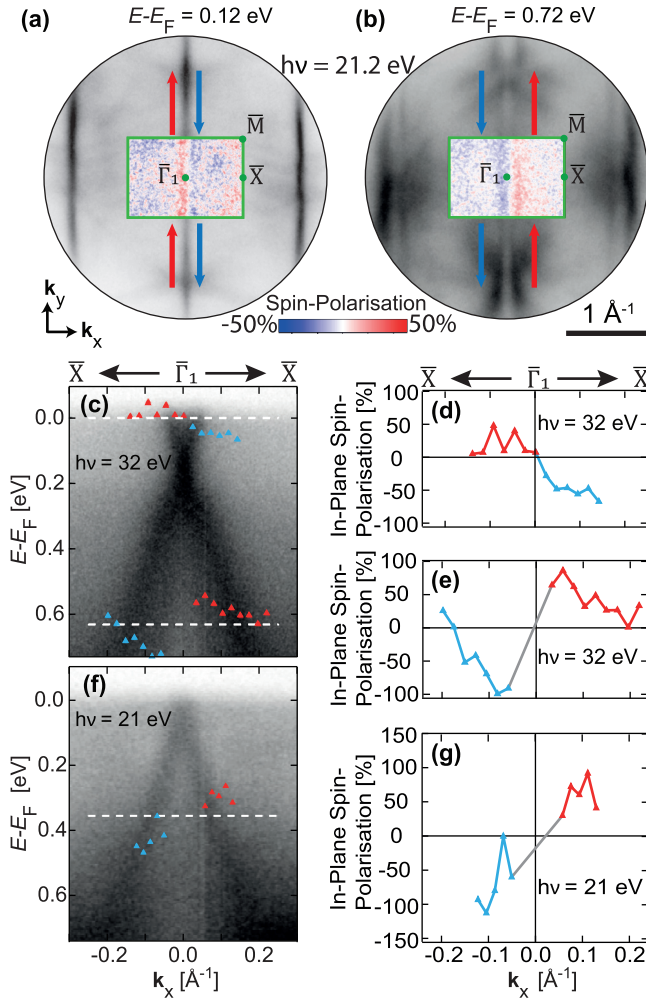
FIG. 4. Measured spin texture. (a), (b) Constant energy surfaces at binding energies $E_B = 0.12$ eV (a) and $E_B = 0.72$ eV (b). The first Brillouin zone is substituted by the in-plane spin polarization along the $\mathbf{k}_y$ direction visualized by red and blue arrows. (c), (f) E_B vs $\mathbf{k}_x$ plot measured with photoexcitation energies of $h\nu = 32$ eV and $h\nu = 21$ eV. The in-plane spin-polarization along $\mathbf{k}_y$ was measured along the dashed white lines and has been overlaid. (d), (e), (g) In-plane spin polarization along $\mathbf{k}_y$ at $E_B = 0$ eV (d) and $E_B = 0.63$ eV (e) in (c), and $E_B = 0.36$ eV (g) in (f).

positive spin polarization (red) occurs for negative values of $\mathbf{k}_x$ (left-hand side of $\bar{\Gamma}_1$), while at $E_B = 0.72$ eV, the positive spin polarization is at positive values of $\mathbf{k}_x$ (right-hand side of $\bar{\Gamma}_1$). This indicates that the spin polarization reverses at a band crossing between $E_B = 0.12 - 0.72$ eV. The spin reversal is confirmed in Figs. 4(c) and 4(f), where the in-plane spin-polarization S_y along the 1D line is overlaid on the E_B vs $\mathbf{k}_x$ maps of the surface states. S_y was found to be $\approx 30\%$ when measured above and below the crossing point for $\times_{0.16\,\mathrm{eV}}$, and $\approx 70\%$ for $\times_{E_F}$, see Figs. 4(d), 4(e), and 4(g), respectively.

It should be noted that the spin texture is similar for both $\times_{E_F}$ and $\times_{0.16\,\mathrm{eV}}$ although their magnitudes differ, as seen when comparing Figs. 4(e) and 4(g). Because of this, we presume that backscattering is strongly reduced for electronic states in the direction corresponding to the atomic chains in Fig. 1(b). In addition, the observed spin polarization means

that instabilities like charge density waves are not expected on the Bi(112) surface [20,31]. This is consistent with the measured LEED pattern as discussed previously.

Signs of an out-of-plane spin-vector component can also be seen when measuring the spin polarization of $\times_{0.16\,\mathrm{eV}}$ [22]. However, this spin-vector component is small compared to S_y, and approaches the detection limit in our measurements. Even though S_z is small in the measurements and is only significant for short $\mathbf{k}_x$ ranges in the calculations, it can explain why the measured S_y in Fig. 4(d) is lower than expected from the calculations. These spin measurements were performed near the Fermi level, which is close to where $\times_{0.16\,\mathrm{eV}}$ and $\times_{E_F}$ cross [yellow/purple circles and purple arrow in Figs. 2(a)–2(c)]. At this point, S_z increases drastically in the calculations and, consequently, S_y decreases.

When comparing the spin polarization found for Bi(112) with Bi(441) and Bi(114) (see Table I), they are found to be similar, but with certain important differences [11,12]. All three surfaces have 1D surface states where the in-plane spin-vector component along $\pm \mathbf{k}_y$ (S_y) is the main component. For $\times_{E_F}$ in Bi(112) and Bi(441), this is the only measurable component. In comparison, $\times_{E_F}$ in Bi(114) and $\times_{0.16\,\mathrm{eV}}$ in Bi(441) were previously found to have an additional out-of-plane component, such that the spin vector makes an angle $\approx 30°$ and $\approx -45°$ relative to the (114) and (441) surface plane, respectively [11,12]. Bianchi *et al.* (2015, Ref. [11]) suggested that the out-of-plane component of the spin may be a consequence of exposing edges of the (111) plane in bismuth (see Fig. 1(a) and the Supplemental Material [22]), and that this spin vector is in fact in plane and parallel to the spin vector of the Bi(111) surface. This would mean that $\times_{E_F}$ in Bi(114) and $\times_{0.16\,\mathrm{eV}}$ in Bi(441) correspond to surface states in Bi(111), while $\times_{E_F}$ in Bi(441) corresponds to surface states on the (441) surface. This hypothesis seems to match well for Bi(441) when comparing the angle of the spin vector with the angle between the (111) and (441) surface planes [11]. Contrary to previous conclusions, the angle of 57° between the Bi(114) and Bi(111) surface planes appear to be larger than the angle of 30° between the Bi(114) surface and its measured spin vector [11,12,22].

To see whether $\times_{E_F}$ and $\times_{0.16\,\mathrm{eV}}$ in Bi(112) can be related to states on different surfaces, their full spin vectors were estimated. As mentioned previously, the spin vector of $\times_{E_F}$ seems to be fully in plane, hence indicating that it belongs to a surface state on Bi(112). On the other hand, $\times_{0.16\,\mathrm{eV}}$ seems to have a small out-of-plane component, resulting in an angle of $(27 \pm 7)°$ between the surface plane and the measured spin vector. This angle is smaller than the 37° miscut angle between the (111) and (112) planes, but almost within the estimated uncertainty. Altogether, the three surfaces have similar spin vectors, but the angles between their surface planes and spin vectors seem to vary. These subtle but important differences potentially mean that the spin vector can be tuned by choosing a particular vicinal surface.

III. CONCLUSION

One-dimensional, spin-polarized surface states have been observed on the (112) surface of bismuth. The surface states are seen as $\times$-like features in the band structure with crossing

points at $E_B = 0.07 \pm 0.10$ eV and $E_B = 0.16 \pm 0.05$ eV for $\times_{E_F}$ and $\times_{0.16\,eV}$, respectively. These values agree with TB calculations within the estimated uncertainties, even if their band gradients differ. The spin vectors of the surface states are mainly in plane and along $\pm\mathbf{k}_y$, but $\times_{0.16\,eV}$ shows indications of having an additional out-of-plane spin-vector component, approximately matching the angle to the (111) plane. The surface states observed in Bi(112) resemble those found for other vicinal surfaces of bismuth, indicating that the existence of such states is a robust property of these surfaces. Furthermore, variations in how the spin vectors tilt out of plane on the different surfaces expand the knowledge of how the electronic and spin structures of low-dimensional surfaces can be modified by adjusting the surface crystallographic direction.

ACKNOWLEDGMENTS

APPENDIX: METHODS

1. Sample preparation

A clean Bi(112) surface was prepared by repeated cycles of Ar^+ ion sputtering at 200-400 eV, followed by annealing to $T \approx 50\,°C$ for a short duration. The cleanliness of the surface was verified by sharp and oxide-free Bi core levels using x-ray photoelectron spectroscopy, and the crystallinty of the surface observed by LEED. Photoemission electron microscopy (PEEM) real-space measurements were utilized to verify that the sample surface was uniform over a larger area.

2. Band-structure and spin measurements

a. Momentum microscopy measurements

Band-structure measurements were performed at $T \approx 115$ K using a NanoESCA III aberration-corrected EF-PEEM, equipped with a focused helium discharge lamp primarily generating He I photons at $h\nu = 21.2$ eV, using a pass energy of $E_P = 25$ eV and a 1.0 mm entrance slit to the energy filter. With the given settings, the instrument had nominal energy and momentum resolutions of approximately 100 meV and $0.02\,Å^{-1}$, respectively.

The uniformity of the sample was further confirmed by obtaining the same band structure at different positions of the sample. The band structure measurements were repeated after shorter and longer time periods (hours, days, months) to ensure that the surface did not change with time. The reproducibility of the bands shows that the observed band structure is from the bismuth itself and not caused by irregularities on the surface or by time-dependent adsorption of impurities.

Two-dimensional spin-polarized measurements at constant energies were performed using an Ir spin-filter coated with a monolayer of gold [32,33]. The spin filter measured the projection of the spin along $\pm\mathbf{k}_y$, i.e., in-plane and along the 1D states. The spin-polarization P was calculated from the measurements using

$$P = \frac{I_\uparrow - I_\downarrow}{S(I_\uparrow + I_\downarrow)}, \qquad (A1)$$

where $I_\uparrow$ and $I_\downarrow$ are the intensities of the energy surface when filtering spin along $+\mathbf{k}_y$ and $-\mathbf{k}_y$, respectively [34]. A Sherman function $S = 0.6$ was assumed based on preliminary calibration measurements [34,35].

b. High-resolution measurements

Higher energy resolution band-structure measurements were performed at the APE-LE end station at Elettra Synchrotron, Italy, using a VG SCIENTA DA30 analyzer while cooling the Bi(112) crystal to $T \approx 77$ K. Measurements were performed at photoexcitation energies between $h\nu = 20 - 85$ eV, in steps of $1 - 5$ eV. $\times_{E_F}$ can be seen at most photoexcitation energies in this range, except for photoexcitation energies between $h\nu = 30 - 35$ eV, where $\times_{0.16\,eV}$ has much higher intensity. Several of these measurements were repeated regularly during two separate weeks to verify that the sample was clean and the measurements consistent.

Spin measurements were performed using two three-dimensional vectorial spin polarimeters operated in the very low-energy electron diffraction (VLEED) regime [36]. From the spin signals detected by the two VLEED spin detectors, it is possible to reconstruct the full three-dimensional spin-vector carried by the emitted photoelectrons. A Sherman function of $S = 0.3$ was found by calibration and was used in the analysis.

3. Calculation details

a. Tight-binding calculations

The bulk band structure of bismuth was calculated within a TB model in Ref. [37]. In this paper, we used the same model and parameters to calculate the band structure of a semi-infinite system with a finite number of layers in the $\hat{\mathbf{z}}$ direction and periodic boundary conditions in the $\hat{\mathbf{x}}\hat{\mathbf{y}}$ plane, where the sample was oriented so the $\hat{\mathbf{x}}\hat{\mathbf{y}}$ plane corresponds to the (112) surface of bismuth. By performing the Fourier transform for the in-plane coordinates, the energy band structure was calculated as eigenvalues of an effective 1D problem at every in-plane momentum vector $\mathbf{k}$. From the eigenvector corresponding to each eigenvalue at a given in-plane momentum, one may extract various properties of the state, such as orbital content, spin, and the spatial distribution in the direction perpendicular to the surface plane. The latter was used to discriminate between bulk and surface states and is the basis for the choice of color in Fig. 2. Within the geometry in the TB calculation, there are two surfaces, which both host surface states. In Fig. 3, however, we only show the surface states corresponding to one of the two surfaces, while the opposing surface contains surface states with opposite spin polarization.

b. DFT calculations

First-principles DFT calculations were carried out to better understand the electronic structure and to further confirm the validity of the TB model. All calculations were carried out with the QUANTUM ESPRESSO DFT package using fully relativistic pseudopotentials and projector augmented-wave exchange-correlation functionals. Bulk calculations were performed with a 40 Ry plane wave cutoff and a convergence threshold of 1×10^{-8} Ry. The **k** points were sampled using a Monkhorst-Pack grid of $12 \times 12 \times 12$ and the lattice constant was found by a relaxation process. In the relaxed structure, the top atomic layer moved slightly into the bulk. Surface states were calculated using a slab geometry with 24 atomic layers and a separation of 15 Å between the slabs. The sampling of **k**-points was done using a Monkhorst-Pack grid of $10 \times 10 \times 1$. The cutoff energy was 40 Ry and the convergence threshold 1×10^{-6} Ry.

[1] A. Hirohata, K. Yamada, Y. Nakatani, I.-L. Prejbeanu, B. Diény, P. Pirro, and B. Hillebrands, Review on spintronics: Principles and device applications, J. Magn. Magn. Mater. **509**, 166711 (2020).

[2] S. Manipatruni, D. E. Nikonov, C.-C. Lin, T. A. Gosavi, H. Liu, B. Prasad, Y.-L. Huang, E. Bonturim, R. Ramesh, and I. A. Young, Scalable energy-efficient magnetoelectric spin-orbit logic, Nature (London) **565**, 35 (2019).

[3] C. Brüne, A. Roth, H. Buhmann, E. M. Hankiewicz, L. W. Molenkamp, J. Maciejko, X.-L. Qi, and S.-C. Zhang, Spin polarization of the quantum spin Hall edge states, Nat. Phys. **8**, 485 (2012).

[4] M. König, S. Wiedmann, C. Brüne, A. Roth, H. Buhmann, L. W. Molenkamp, X.-L. Qi, and S.-C. Zhang, Quantum spin Hall insulator state in HgTe quantum wells, Science **318**, 766 (2007).

[5] P. Roushan, J. Seo, C. V. Parker, Y. S. Hor, D. Hsieh, D. Qian, A. Richardella, M. Z. Hasan, R. J. Cava, and A. Yazdani, Topological surface states protected from backscattering by chiral spin texture, Nature (London) **460**, 1106 (2009).

[6] H. C. Koo, J. H. Kwon, J. Eom, J. Chang, S. H. Han, and M. Johnson, Control of spin precession in a spin-injected field effect transistor, Science **325**, 1515 (2009).

[7] L. Bawden, J. M. Riley, C. H. Kim, R. Sankar, E. J. Monkman, D. E. Shai, H. I. Wei, E. B. Lochocki, J. W. Wells, W. Meevasana, T. K. Kim, M. Hoesch, Y. Ohtsubo, P. Le Fèvre, C. J. Fennie, K. M. Shen, F. Chou, and P. D. C. King, Hierarchical spin-orbital polarization of a giant Rashba system, Sci. Adv. **1**, e1500495 (2015).

[8] Ph. Hofmann, The surfaces of bismuth: Structural and electronic properties, Prog. Surf. Sci. **81**, 191 (2006).

[9] R. Noguchi, T. Takahashi, K. Kuroda, M. Ochi, T. Shirasawa, M. Sakano, C. Bareille, M. Nakayama, M. D. Watson, K. Yaji, A. Harasawa, H. Iwasawa, P. Dudin, T. K. Kim, M. Hoesch, V. Kandyba, A. Giampietri, A. Barinov, S. Shin, R. Arita *et al.*, A weak topological insulator state in quasi-one-dimensional bismuth iodide, Nature (London) **566**, 518 (2019).

[10] G. Autès, A. Isaeva, L. Moreschini, J. C. Johannsen, A. Pisoni, R. Mori, W. Zhang, T. G. Filatova, A. N. Kuznetsov, L. Forró, W. Van den Broek, Y. Kim, K. S. Kim, A. Lanzara, J. D. Denlinger, E. Rotenberg, A. Bostwick, M. Grioni, and O. V. Yazyev, A novel quasi-one-dimensional topological insulator in bismuth iodide β-Bi$_4$I$_4$, Nat. Mater. **15**, 154 (2016).

[11] M. Bianchi, F. Song, S. Cooil, Å. F. Monsen, E. Wahlström, J. A. Miwa, E. D. L. Rienks, D. A. Evans, A. Strozecka, J. I. Pascual, M. Leandersson, T. Balasubramanian, Ph. Hofmann, and J. W. Wells, One-dimensional spin texture of Bi(441): Quantum spin Hall properties without a topological insulator, Phys. Rev. B **91**, 165307 (2015).

[12] J. W. Wells, J. H. Dil, F. Meier, J. Lobo-Checa, V. N. Petrov, J. Osterwalder, M. M. Ugeda, I. Fernandez-Torrente, J. I. Pascual, E. D. L. Rienks, M. F. Jensen, and Ph. Hofmann, Nondegenerate metallic states on Bi(114): A one-dimensional topological metal, Phys. Rev. Lett. **102**, 096802 (2009).

[13] D. Hsieh, Y. Xia, L. Wray, D. Qian, A. Pal, J. H. Dil, J. Osterwalder, F. Meier, G. Bihlmayer, C. L. Kane, Y. S. Hor, R. J. Cava, and M. Z. Hasan, Observation of unconventional quantum spin textures in topological insulators, Science **323**, 919 (2009).

[14] Y. Xia, D. Qian, D. Hsieh, L. Wray, A. Pal, H. Lin, A. Bansil, D. Grauer, Y. S. Hor, R. J. Cava, and M. Z. Hasan, Observation of a large-gap topological-insulator class with a single Dirac cone on the surface, Nat. Phys. **5**, 398 (2009).

[15] Y. L. Chen, J. G. Analytis, J.-H. Chu, Z. K. Liu, S.-K. Mo, X. L. Qi, H. J. Zhang, D. H. Lu, X. Dai, Z. Fang, S. C. Zhang, I. R. Fisher, Z. Hussain, and Z.-X. Shen, Experimental realization of a three-dimensional topological insulator, Bi$_2$Te$_3$, Science **325**, 178 (2009).

[16] Z.-H. Pan, E. Vescovo, A. V. Fedorov, D. Gardner, Y. S. Lee, S. Chu, G. D. Gu, and T. Valla, Electronic structure of the topological insulator Bi$_2$Se$_3$ using angle-resolved photoemission spectroscopy: Evidence for a nearly full surface spin polarization, Phys. Rev. Lett. **106**, 257004 (2011).

[17] J. W. Wells, K. Handrup, J. F. Kallehauge, L. Gammelgaard, P. Bøggild, M. B. Balslev, J. E. Hansen, P. R. E. Petersen, and Ph. Hofmann, The conductivity of Bi(111) investigated with nanoscale four point probes, J. Appl. Phys. **104**, 053717 (2008).

[18] H. Guo, K. Sugawara, A. Takayama, S. Souma, T. Sato, N. Satoh, A. Ohnishi, M. Kitaura, M. Sasaki, Q.-K. Xue, and T. Takahashi, Evolution of surface states in Bi$_{1-x}$Sb$_x$ alloys across the topological phase transition, Phys. Rev. B **83**, 201104(R) (2011).

[19] X.-G. Zhu and Ph. Hofmann, Topological surface states on Bi$_{1-x}$Sb$_x$: Dependence on surface orientation, termination, and stability, Phys. Rev. B **89**, 125402 (2014).

[20] T. K. Kim, J. Wells, C. Kirkegaard, Z. Li, S. V. Hoffmann, J. E. Gayone, I. Fernandez-Torrente, P. Häberle, J. I. Pascual, K. T. Moore, A. J. Schwartz, H. He, J. C. H. Spence, K. H. Downing, S. Lazar, F. D. Tichelaar, S. V. Borisenko, M. Knupfer, and Ph. Hofmann, Evidence against a charge density wave on Bi(111), Phys. Rev. B **72**, 085440 (2005).

[21] Ph. Hofmann, M. M. Ugeda, A. Tamtogl, A. Ruckhofer, W. E. Ernst, G. Benedek, A. J. Martínez-Galera, A. Stróżecka, J. M. Gómez-Rodríguez, E. Rienks, M. F. Jensen, J. I. Pascual,

and J. W. Wells, Strong-coupling charge density wave in a one-dimensional topological metal, Phys. Rev. B **99**, 035438 (2019).

[22] See Supplemental Material at http://link.aps.org/supplemental/10.1103/PhysRevB.108.205403, which includes Refs. [11,12,21,26,38–42] for details of the LEED analysis, the DFT calculations compared to the TB calculations and the measurements, the one-dimensionality of the surface states and how the binding energy of their crossing points were found, the orbital nature of the electronic states, details regarding the measured out-of-plane spin component, the spin-vector, and the initial state spin polarization, and a comparison of Bi(112) with Bi(111), Bi(441), and Bi(114).

[23] A. Damascelli, Probing the electronic structure of complex systems by ARPES, Phys. Scr. **T109**, 61 (2004).

[24] S. D. Kevan and W. Eberhardt, *Angle-Resolved Photoemission: Theory and Current Applications*, edited by S. D. Kevan (Elsevier, Amsterdam, 1992), Chap. 4.

[25] R. P. Day, B. Zwartsenberg, I. S. Elfimov, and A. Damascelli, Computational framework chinook for angle-resolved photoemission spectroscopy, npj Quantum Mater. **4**, 54 (2019).

[26] J. Bakkelund, Investigating spin-split surface states on semimetals and correlation effects in a ferromagnet, Master's thesis, Norwegian University of Science and Technology, https://hdl.handle.net/11250/3007070 (2022).

[27] J. N. Crain, J. L. McChesney, F. Zheng, M. C. Gallagher, P. C. Snijders, M. Bissen, C. Gundelach, S. C. Erwin, and F. J. Himpsel, Chains of gold atoms with tailored electronic states, Phys. Rev. B **69**, 125401 (2004).

[28] N. W. Ashcroft and N. D. Mermin, *Solid State Physics* (Holt, Rinehart and Winston, New York, 1976), Chap. 1.

[29] C. Kittel and P. McEuen, *Introduction to Solid State Physics* (John Wiley & Sons, Hoboken, NJ, 2018), Chap. 15.

[30] J. Viernow, J.-L. Lin, D. Y. Petrovykh, F. M. Leibsle, F. K. Men, and F. J. Himpsel, Regular step arrays on silicon, Appl. Phys. Lett. **72**, 948 (1998).

[31] D. Leuenberger, H. Yanagisawa, S. Roth, J. H. Dil, J. W. Wells, Ph. Hofmann, J. Osterwalder, and M. Hengsberger, Excitation of coherent phonons in the one-dimensional Bi(114) surface, Phys. Rev. Lett. **110**, 136806 (2013).

[32] C. Tusche, A. Krasyuk, and J. Kirschner, Spin resolved bandstructure imaging with a high resolution momentum microscope, Ultramicroscopy Special Issue: LEEM-PEEM 9, **159**, 520 (2015).

[33] J. Kirschner, F. Giebels, H. Gollisch, and R. Feder, Spin-polarized electron scattering from pseudomorphic Au on Ir(001), Phys. Rev. B **88**, 125419 (2013).

[34] F. Meier, J. H. Dil, and J. Osterwalder, Measuring spin polarization vectors in angle-resolved photoemission spectroscopy, New J. Phys. **11**, 125008 (2009).

[35] N. Sherman, Coulomb scattering of relativistic electrons by point nuclei, Phys. Rev. **103**, 1601 (1956).

[36] C. Bigi, P. K. Das, D. Benedetti, F. Salvador, D. Krizmancic, R. Sergo, A. Martin, G. Panaccione, G. Rossi, J. Fujii, and I. Vobornik, Very efficient spin polarization analysis (VESPA): New exchange scattering-based setup for spin-resolved ARPES at APE-NFFA beamline at Elettra, J. Synchrotron Radiat. **24**, 750 (2017).

[37] Y. Liu and R. E. Allen, Electronic structure of the semimetals Bi and Sb, Phys. Rev. B **52**, 1566 (1995).

[38] Single Crystal 4, Crystal Maker Software Limited, https://crystalmaker.com/singlecrystal/ (2022).

[39] F. J. Himpsel, Experimental determination of bulk energy band dispersions, Appl. Opt. **19**, 3964 (1980).

[40] B. Singh, R. Hesse, and M. Linford, Good practices for XPS (and other types of) peak fitting. Use chi squared, use the abbe criterion, show the sum of fit components, show the (normalized) residuals, choose an appropriate background, estimate fit parameter uncertainties, limit the number of fit parameters, use information from other techniques, and use common sense, Vac. Technol. Coating 25 (2015).

[41] S. Cho, S. Huh, Y. Fang, C. Hua, H. Bai, Z. Jiang, Z. Liu, J. Liu, Z. Chen, Y. Fukushima, A. Harasawa, K. Kawaguchi, S. Shin, T. Kondo, Y. Lu, G. Mu, F. Huang, and D. Shen, Supporting information for "Direct observation of the topological surface state in the topological superconductor 2M-WS2," Nano Lett. **22**, 8827 (2022).

[42] J. Henk, K. Miyamoto, and M. Donath, Retrieving the initial-state spin polarization from spin-resolved photoemission: Proposal for a case study on W(110), Phys. Rev. B **98**, 045124 (2018).